Journal of Magnetic Resonance 212 (2011) 204–215

Contents lists available at ScienceDirect

Journal of Magnetic Resonance

journal homepage: www.elsevier.com/locate/jmr

BaBa-xy16: Robust and broadband homonuclear DQ recoupling for applications in rigid and soft solids up to the highest MAS frequencies ☆

Kay Saalwächter [a,*], Frank Lange [a], Krzysztof Matyjaszewski [b], Chih-Feng Huang [b], Robert Graf [c,*]

[a] Institut für Physik – NMR, Martin-Luther-Universität Halle-Wittenberg, Betty-Heimann-Str. 7, D-06120 Halle, Germany
[b] Department of Chemistry, Carnegie Mellon University, 4400 Fifth Avenue, Pittsburgh, PA 15213, United States
[c] Max-Planck-Institute for Polymer Research, Ackermannweg 10, D-55128 Mainz, Germany

ARTICLE INFO

Article history:
Received 18 April 2011
Revised 28 June 2011
Available online 12 July 2011

Keywords:
Multiple-quantum NMR
Double-quantum NMR
Recoupling
^{31}P NMR
Phosphates
Polymers
Elastomers
Networks
Biomolecular solid-state NMR

ABSTRACT

We here present a substantially improved version of the popular Back-to-Back (BaBa) homonuclear double-quantum (DQ) MAS recoupling pulse sequence. By combining the original pulse sequence with a virtual π pulse train with xy-16 phase cycling along with time-reversed DQ reconversion, a truly broadband and exceptionally robust pulse sequence is obtained. The sequence has moderate radio-frequency power requirements, amounting to only one 360° nutation per rotor cycle, it is robust with respect to rf power and tune-up errors, and its broadband performance increases with increasing spinning frequency, here tested up to 63 kHz. The experiment can be applied to many spin-1/2 nuclei in rigid solids with substantial frequency offsets and CSAs, which is demonstrated on the example of ^{31}P NMR of a magnesium ultraphosphate, comparing experimental data with multi-spin simulations, and we also show simulations addressing the performance in ^{13}C NMR of bio(macro)molecules. ^{1}H-based studies of polymer dynamics are highlighted for the example of a rigid solid with strongly anisotropic mobility, represented by a polymer inclusion compound, and for the example of soft materials with weak residual dipole–dipole couplings, represented by homogeneous and inhomogeneous elastomers. We advocate the use of normalized (relaxation-corrected) DQ build-up curves for a quantitative assessment of weak average dipole–dipole couplings and even distributions thereof.

1. Introduction

The precise measurement of dipole–dipole coupling constants (DCCs) between NMR-active nuclei is still one of the major goals in modern solid-state NMR method development. Dipole–dipole couplings precisely reflect internuclear distances as well as dynamics on time scales of the inverse coupling constant and faster. In the domain of fast averaging, a potential anisotropy of the motion is directly reflected by the reduced (residual) dipolar coupling constant (RDCC). We here address the determination (or at least estimation) of homonuclear dipole–dipole couplings under high-resolution magic-angle spinning (MAS) conditions, for which a large variety of recoupling pulse sequences have been developed. We focus on pulse sequences that excite double-quantum (DQ) coherences, since these naturally reflect the DCCs between the spins involved in terms of well-quantifiable DQ build-up data, taken as a function of pulse sequence (recoupling) time. They further allow for the acquisition of 2D correlation spectra that are free of the often dominant spectral diagonal that is present in conventional 2D single-quantum (SQ) exchange-type spectra [1]. All signals from uncoupled spins reside in this diagonal and often deteriorate the resolution, a complication easily avoided in DQ–SQ correlation spectra.

Starting with the "dipolar recoupling at the magic angle" (DRAMA) experiment by Tycko [2] as one of the earliest DQ MAS pulse sequences published two decades ago, many improvements towards robustness and broadband excitation have been reported in the years that followed [3]. Levitt's symmetry theory [4,5] provided a rational basis for pulse sequence design that led to many powerful pulse sequences, of which C7 [6], and in particular its better compensated (permutationally offset stabilized) companion POST-C7 [7], henceforth referred to as pC7, are among the best-known and often-used examples.

One major challenge that has been addressed in recent years is the use of higher MAS frequencies, where dipolar recoupling during finite π pulses [8], termed finite-pulse radio-frequency driven recoupling (fpRFDR) proved applicable at 20 kHz and beyond, and can also be combined with DQ excitation by adding properly

☆ Revised version, submitted to J. Magn. Reson.

* Corresponding authors.
E-mail addresses: kay.saalwaechter@physik.uni-halle.de (K. Saalwächter), graf@mpip-mainz.mpg.de (R. Graf).
URL: http://www.physik.uni-halle.de/nmr (K. Saalwächter).

1090-7807/$ - see front matter © 2011 Elsevier Inc. All rights reserved.
doi:10.1016/j.jmr.2011.07.001

spaced 90° pulses [9]. DQ MAS spectroscopy based on fpRFDR proved applicable at the highest MAS frequencies available to date (~70 kHz), and was recently compared with other pulse sequences [10–12], including a promising new variant termed SPIP (sandwiched pi pulse scheme). Applying such modern pulse sequences to challenging systems with large offsets and CSAs, such as ^{31}P or ^{19}F, DQ efficiencies of up to 0.35 (as compared to the total SQ signal) have been reported [11–13]. Another line of new developments concerns pulse sequences with low power requirements and simpler average spin Hamiltonians (isotropic mixing), which can be obtained by numerical optimization schemes [14,15]. A final, yet unsolved quantum-mechanical challenge is the difficulty in measuring weak pair couplings in the presence of stronger ones, referred to as dipolar truncation. The phenomenon was studied by theory and simulations [16], and can so far only be circumvented by suitable isotope labelling schemes.

In this contribution, we come back to one of the earliest shift-compensated DQ recoupling sequences, namely Back-to-Back (BaBa) published by Feike et al. [17]. Recognized for its utter simplicity, consisting of 4 90° pulses per rotor period (τ_R), BaBa is clearly one of the most popular DQ pulse sequences, and has mainly been used in ^{1}H DQ fast-MAS spectroscopy with 25 kHz spinning or above [18,19]. As per its symmetry properties, BaBa is closely related to DRAMA, and was developed in addressing the missing shift compensation of the latter. Even though BaBa was experimentally introduced in its application to ^{31}P with large CSA for the elucidation of coupling networks in phosphates [20], its "broadband" version was explicitly addressed for its comparably poor performance at large offsets or CSA [11,12].

We here remedy this shortcoming by introducing a truly broadband BaBa variant based on rational design principles. A similar approach was recently published for the DRAMA experiment [21], yet at the expense of introducing additional finite-length π pulses, thus complicating the tune-up and not reaching offset compensation in excess of a few kHz. Our approach consists in adding virtual π pulses, simply leading to changes in the pulse phases, as already done for the first compensation efforts for BaBa [17]. Our variant essentially arises from a combination with the xy-16 supercycle developed for long π pulse trains [22], thus the name BaBa-xy16.

In taking advantage of the improved long-time performance of BaBa-xy16, we advocate the use of point-by-point normalized (relaxation-corrected) DQ build-up curves as a reliable way to measure (R)DCCs. While constant-time approaches [8,23] also have the feature of being free of relaxation effects, taking DQ build-up and suitable reference data for use in point-by-point normalization has the additional benefit that the magnitude of "relaxation", i.e., coherence decay arising from pulse sequence imperfections, higher-order Hamiltonian contributions, or actual intermediate motions, can be quantified directly. Further, the fraction of spins involved in the coupling network can be quantified exactly, since intensities are directly referenced to the total signal of the sample, where a fraction of nuclei may not be coupled. This prevents the undesirable effect of addressing not properly quantified and potentially non-representative sub-ensembles in complex inhomogeneous materials. Further, we will demonstrate the possibility to extract not only average (R)DCCs, but also distributions in inhomogeneous systems by analysis of the shape of normalized DQ (nDQ) build-up curves. According to our experience, the shape of constant-time modulation curves proved much less sensitive to distribution effects than the shape of nDQ build-up curves. For the case of a homogeneous multi-spin system, the latter can be described by a generic empirical function.

2. Experimental

2.1. Samples

The performance of the experiment for the case of large CSAs and comparably weak ^{31}P–^{31}P dipole–dipole couplings is demonstrated on magnesium ultraphosphate MgP_4O_{11}. In order to reduce its excessively long T_1, the sample was doped with a small amount of Co^{2+} located at the Mg site by addition of a corresponding salt during synthesis; it was the same sample as studied by Feike et al. [17]. An inclusion compound of poly(dimethysiloxane), PDMS, of 2.6 kg/mol molecular weight in long channel-like cavities formed by stacked γ-cyclodextrin rings was the same one as investigated earlier [24], and serves as an example for the determination of comparably strong yet motionally averaged ^{1}H–^{1}H dipole–dipole couplings.

Weak but well-defined ^{1}H–^{1}H dipole–dipole couplings are present in long-chain entangled polymer melts, and in permanently cross-linked elastomers (rubbers), as a result of locally anisotropic chain motion, as arising from topological constraints [25]. We demonstrate the use of DQ NMR in the area of soft materials on the example of a natural rubber (NR) sample, vulcanized with a conventional cure system containing by weight 3.1 parts sulfur per 100 parts rubber. Details on the sample are published in Ref. [26]. Conventionally vulcanized NR is generally a very homogeneous material, characterized by a well-defined RDCC and a narrow distribution. A more challenging case with an inhomogeneous distribution of RDCCs is represented by a poly(methyl acrylate) (PMA) model network, prepared by cross-linking of 4-arm star precursor polymers made by ATRP polymerization [27–30], with a molecular weight of 13.3 kg/mol (37 monomers per arm). The arm ends were functionalized by azide groups and connected via "click"-reaction with a propargyl ether as difunctional cross-link in 6.5 molar solution in DMF (corresponding to a volume swelling degree of 4.35). After cross-linking, the gel was dried and re-swollen to a volume swelling degree of 1.5 in THF-d_8 and flame-sealed in a small glass tube fitting a 4 mm MAS rotor, in order to prevent evaporation and enable sample temperatures above the boiling point of THF. Solvent swelling is necessary in this case in order to decrease the glass transition temperature of PMA, since DQ NMR on networks needs to be carried out far above T_g in order to ensure fast-limit averaging conditions over all possible network chain conformations between the cross-linking points [25,26].

2.2. NMR experiments

NMR experiments were carried out on a Bruker Avance III wide-bore 400 MHz spectrometer equipped with a 4 mm double-resonance MAS probe, and on a Bruker Avance III standard-bore 600 MHz instrument equipped with 2.5 mm and 1.3 mm double-resonance MAS probes providing spinning frequencies of up to 30 and 63 kHz, respectively. ^{1}H chemical shifts for the elastomer studies at 400 MHz were referenced to the known resonances of NR [31], ^{31}P shifts were set to the known shifts of MgP_4O_{11} [17], and ^{1}H shifts under fast-MAS conditions at 600 MHz were externally referenced to alanine. The elastomers at 400 MHz were studied at elevated temperature using a Bruker BVT 3000 system based on heated air, and the reported actual sample temperatures are based on a suitable calibration. No temperature control was used for the fast-MAS experiments, which means that sample temperatures were about 45 and 70 °C at 30 and 60 kHz spinning, respectively. Unless noted otherwise, the 90° pulse lengths for the given nuclei were typically set to 3, 1.6 and 1.3 μs on the 4, 2.5 and 1.3 mm MAS probes, respectively. The NR sample was also (re)-measured with a static DQ pulse sequence [32,33] on a 20 MHz

Bruker minispec following previously published procedures [25,26].

2.3. Spin dynamics simulations

Spin dynamics simulations of the ^{31}P NMR response of MgP_4O_{11}, considering the full BaBa sequence with finite pulses including all explicit pulse phases and the full double-quantum and reference selection phase cycles were carried out using the SPINEVOLUTION software [34]. The simulations were based on the known crystal structure of MgP_4O_{11} [35] and the published chemical-shift anisotropies of the ^{31}P resonances [17,36]. Recent ab-initio calculations indicate that the orientations of the CSA principal components lie along the chemically intuitive symmetry directions with only small deviations of a few degrees [36,37]. Overall, we found that the simulation results were only weakly dependent on the CSA orientations.

3. Theory and pulse sequence design

DQ, or more generally multiple-quantum (MQ) NMR addressing all even quantum orders in multi-spin systems [38], is most efficiently done with a pulse sequence producing a pure DQ average Hamiltonian,

$$\widehat{H}_{\mathrm{DQ}} = \sum_{j<i}^{\text{all spins}} b^{ij}\left\{\widehat{T}^{ij}_{2,2} + \widehat{T}^{ij}_{2,-2}\right\} = \sum_{j<i}^{\text{all spins}} b^{ij}\left\{\widehat{H}^{ij}_{xx} - \widehat{H}^{ij}_{yy}\right\}. \tag{1}$$

Restricting the formalism for the moment to an isolated spin pair, the prefactor b for static MQ NMR using the pulse sequence of Baum and Pines [32,33] reads

$$b_{\mathrm{stat}} = D\, P_2(\cos\theta), \tag{2}$$

where D is the DCC in rad/s (2π s^{-1}), and θ is the polar angle denoting the pair vector orientation with respect to B_0. For the BaBa DQ MAS recoupling sequence [17] we have

$$b_{\mathrm{BaBa}} = \left(\frac{3}{\pi\sqrt{2}}\right) D \sin 2\beta \sin\gamma \tag{3}$$

where β and γ are the Euler angles locating the spin pair vector in the rotor frame. We note that the BaBa Hamiltonian and thus the final signal function has the same dependence on the orientation angles as REDOR, the probably most famous heteronuclear recoupling method [39]. This is not a coincidence, as both sequences are ultimately based on an inversion of the spin Hamiltonian under MAS during every other half rotor period.

In a pulse sequence consisting of excitation and reconversion periods of equal length τ_{DQ} followed by a read-out pulse, the common 4-step DQ selection phase cycle [1] consisting of the rotation of the excitation or reconversion base phase in 90° steps and an alternation of the receiver between ±180° yields the powder-averaged signal

$$I_{\mathrm{DQ}} = \langle \sin^2\phi \rangle, \tag{4}$$

for which we define a dipolar phase factor $\phi = \int_0^{\tau_{\mathrm{DQ}}} b(t)\mathrm{d}t$ Note that even when $b(t)$ is defined as a prefactor characterizing a MAS-period-averaged Hamiltonian, it may be time-dependent due to molecular motion on longer time scales. In samples without mobility, $\phi = b\tau_{\mathrm{DQ}}$. Without receiver alternation, one obtains a reference signal

$$I_{\mathrm{ref}} = \langle \cos^2\phi \rangle \tag{5}$$

which for the case of a spin pair corresponds to modulated longitudinal magnetization (quantum order 0). Obviously, both functions approach a relative signal level of 0.5 in the long-time limit, adding up to the complete initial magnetization. A suitable signal function which shows no time modulation due to dipolar couplings and which can be used for a point-by-point normalization correcting for true motion-related relaxation effects, pulse sequence imperfections, or higher-order dephasing terms, is the sum function

$$I_{\Sigma\mathrm{MQ}} = I_{\mathrm{DQ}} + I_{\mathrm{ref}} = \langle \sin^2\phi \rangle + \langle \cos^2\phi \rangle. \tag{6}$$

Note that except in the fast-motion limit (rate constant $k \ll D^{-1}$), the decay of $I_{\Sigma\mathrm{MQ}}$ due to intermediate motions or higher-order dephasing is never exponential. Good fits to experimental data are often obtained using a stretched or compressed exponential function, $\exp\left\{-(2\tau_{\mathrm{DQ}}/T_2^*)^{\beta}\right\}$ with β ranging from ~0.5 to 2.

The normalized DQ (nDQ) build-up function is then

$$I_{\mathrm{nDQ}} = I_{\mathrm{DQ}}/(I_{\Sigma\mathrm{MQ}} - \mathit{tails}), \tag{7}$$

where one may have to subtract the contribution of uncoupled spins that usually contribute a slowly relaxing, often exponential signal *tail* in I_{ref} and thus in $I_{\Sigma\mathrm{MQ}}$ (see Fig. 9 below for an example). After normalization, the I_{nDQ} function thus approaches the relative intensity of 0.5 in the long-time limit. This still holds for multi-spin systems, where the DQ Hamiltonian excites all even quantum orders. These are equally shared among the I_{DQ} and I_{ref} signal functions, which given the 4-step selection phase cycle contain all $4n+2$ and $4n$ coherence orders, respectively. $I_{\Sigma\mathrm{MQ}}$ is thus formally a perfect multi-spin dipolar echo function as long as unwanted odd-order coherences are not excited. In few-spin systems the intensity plateau can differ, e.g., it is 1/3 for the case of ^{1}H DQ spectroscopy on an isolated methyl group [33]. In the multi-spin case, if all species have very close resonance frequencies (or when the spinning rate is high enough to refocus shift differences on a sufficiently short timescale), the apparent dipolar coupling is a second-moment-type quantity

$$D_{\mathrm{app}} = \left(\sum_{j<i}^{\text{all spins}} D_{ij}^2\right)^{1/2}. \tag{8}$$

Previous spin-counting experiments and multi-spin simulations have shown that the initial build-up of I_{nDQ} is always dominated by DQ coherences, meaning that a well-defined D_{app} can be obtained by fitting the initial rise.

The validity of Eq. (8) deserves a few comments. It is well-applicable in systems with a spatially homogeneous distribution of spins, such as dense protons in organic solids [18] or the phosphate network structure discussed below. It should still work well in systems with a large dominant pair interaction and weaker secondary couplings, where of course only the dominant coupling is accessible and reflected in D_{app}. The approximation is expected to break down in case of a rather isolated spin that is coupled to many other spins that are themselves coupled strongly among each other. Then, the dipolar truncation effect [16] would complicate the spin dynamics and lead to an underestimated D_{app}. Additionally, in a spin system with weak couplings and large shift differences (or large CSAs and non-colinear tensor orientations), second-averaging introduces the well-known factor of 2/3 for the coupling constants (heteronuclear limit). It should, however, be noted that for moderate shift differences, this effect can be partially compensated by sufficiently fast shift refocussing, as provided by faster spinning with the given chemical-shift compensated pulse sequence.

A simple fitting function for $I_{\mathrm{nDQ}}(\tau_{\mathrm{DQ}})$ can be obtained via a second-moment approximation [25,40,41]. Neglecting intensity relaxation,

$$I_{\mathrm{nDQ}} \approx \langle \sin^2\phi \rangle \approx \frac{1}{2}\left\{1 - e^{-2\langle\phi^2\rangle}\right\}. \tag{9}$$

Now, the powder averaging is to be performed over the square phase factor, which is a straightforward exercise, yielding

$$\langle\phi^2\rangle_{\mathrm{stat}} = D^2\tau_{\mathrm{DQ}}^2\frac{1}{2}\int_0^{\pi} P_2(\cos\theta)^2\sin\theta \mathrm{d}\theta = \frac{1}{5}D^2\tau_{\mathrm{DQ}}^2 \tag{10}$$

for the static case [25,33] and

$$\langle\phi^2\rangle_{\mathrm{BaBa}} = \frac{9}{2\pi^2}D^2\tau_{\mathrm{DQ}}^2\frac{1}{4\pi}\int_0^{2\pi}\int_0^{\pi}\sin^2 2\beta\sin^2\gamma\sin\beta \mathrm{d}\beta\mathrm{d}\gamma = \frac{9}{2\pi^2}D^2\tau_{\mathrm{DQ}}^2\frac{4}{15} = \frac{6}{5\pi^2}D^2\tau_{\mathrm{DQ}}^2 \tag{11}$$

for BaBa, where of course τ_{DQ} can only be incremented in full rotor periods $N\tau_{\mathrm{R}}$. In Fig. 1 the approximations are compared to the powder-averaged signal functions. Obviously, Eq. (9) is a good approximation up to $I_{\mathrm{nDQ}} \approx 0.3$, and it provides even better fits in multi-spin systems [25,33]. Comparing Eqs. (10) and (11), we see that the DQ build-up under BaBa is only slightly (by a factor of $\sqrt{6/\pi^2} = 0.78$) less efficient than in the static case.

Concluding this part, we stress that it is the removal of intensity relaxation effects by point-by-point normalization with $I_{\Sigma\mathrm{MQ}}$ which establishes an absolute intensity scale and opens the possibility to use Eq. (9) to determine the dominant, or (in a homogeneous multi-spin system) apparent average coupling constant associated with a given nucleus by a simple fit to the initial rise. This represents a true advantage over the analysis of the oscillations at longer times, as these are, first, much more sensitive to the unknown spin system topology (deviations from the spin-pair scenario), and are, second, measured less accurately due to the overall intensity relaxation.

We note that the dominating factors for the overall signal decay reflected in $I_{\Sigma\mathrm{MQ}}$ are in most cases experimental imperfections and deleterious higher-order contributions in the average Hamiltonian, which become important if the spin interactions (dipole–dipole couplings and CSA) are on the order of or larger than the inverse cycle time ($\sim\omega_{\mathrm{R}}$). In contrast, when the interactions are small, the decay of $I_{\Sigma\mathrm{MQ}}$ (and also the long-time decay of I_{DQ}) reflects true transverse relaxation (T_2) effects due to motions on the timescale of D^{-1}. This limit is realized in mobile soft materials with anisotropic mobility (polymers, liquid crystals), which are characterized by rather weak ^{1}H RDCCs on the order of a few hundred Hz or less. In this case, second-moment (Anderson–Weiss) based theory [40] can be used to describe the decay functions quantitatively in terms of realistic dynamic models for chains in elastomers [25,42] or entangled polymer melts [43]. Such fully quantitative studies on static samples can further be performed on simple low-field equipment. In the Results section, we will show experimental comparisons between DQ excitation curves taken on static samples and under MAS, using BaBa and pC7.

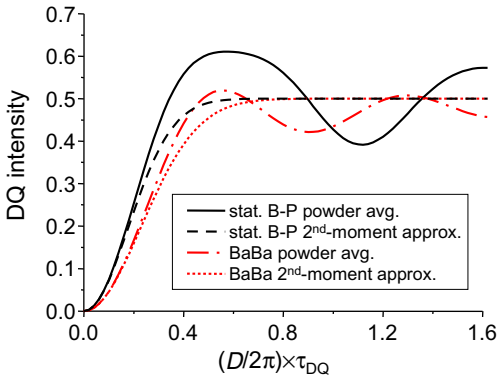

Fig. 1. Comparison of the powder-averaged signal functions, Eq. (4), with the second-moment approximations, Eq. (9), using in each case the pulse-sequence specific phase factors $\phi = b\tau_{\mathrm{DQ}}$. Note the normalized x-axis.

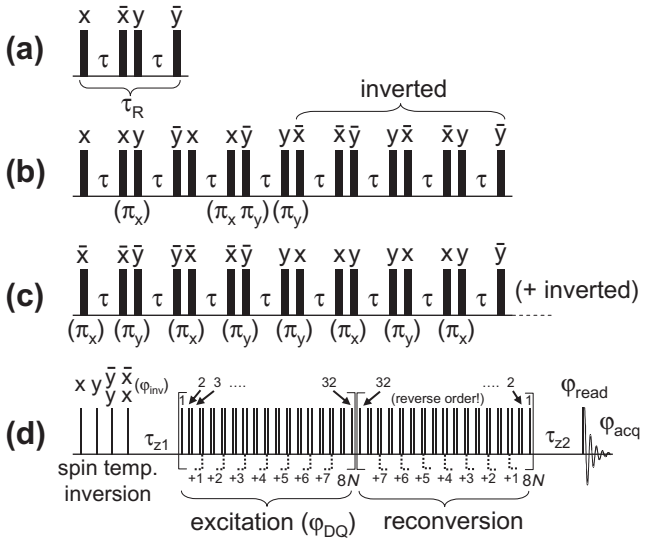

Fig. 2. BaBa pulse sequences as described in the text. (a) BaBa basic cycle, (b) "broadband" BaBa [17], and (c) BaBa-xy16. In (d), the full DQ experiment is shown, consisting of preparation (phase-cycle controlled spin-temperature inversion based on composite pulses), DQ excitation with base phase φ_{DQ}, DQ reconversion, and read-out. All black bars denote 90° pulses.

We now address the proper shift/offset compensation of the BaBa sequence, which was already addressed by Feike et al. [17]. The basic BaBa cycle is depicted in Fig. 2a. In Fig. 2b the then-recommended and most popular "broadband" BaBa is shown, which consists of a supercycle of $4\tau_{\mathrm{R}}$ length. Some of the pulse phases are inverted, based on the concept of virtual 180° pulses located between the pulse pairs flanking the $0.5\tau_{\mathrm{R}}$ free-evolution intervals. For instance, $90^\circ_x 90^\circ_{\bar{y}}$ corresponds to $90^\circ_{\bar{x}}\left(180^\circ_x 180^\circ_y\right)90^\circ_y$. The virtual π pulses are shown in brackets below the sequence. The sequence in Fig. 2b removes offset and chemical-shift effects to first order, yet Feike et al. did not give any motivation for the placement of the compensating π pulses.

A more rational design attempt is to include the well-known xy-16 phase cycling that was developed for improving the long-time performance of π pulse trains [22], and which is successfully applied in REDOR experiments to measure weak heteronuclear dipole–dipole couplings. Our BaBa-xy16 variant is shown in Fig. 2c. The shown $4\tau_{\mathrm{R}}$ cycle includes a virtual π pulse train with *xyxyyxyx* phases, which corresponds to xy-8 [22]. For xy-16, this sequence is repeated in inverted form. Noting that $90^\circ_{\bar{x}} = 90^\circ_x(180^\circ_x) = 90^\circ_x(180^\circ_{\bar{x}})$, meaning that the virtual-pulse concept does not distinguish the π pulse sign, we repeat the whole BaBa-xy8 block in phase-inverted form to obtain the full $8\tau_{\mathrm{R}}$ cycle consisting of 32 90° pulses.

Our aim was to develop a sequence that would provide DQ build-up points in as-small-as-possible increments, best in steps of $1\tau_{\mathrm{R}}$. The most robust implementation is shown in Fig. 2d, which indicates that the best way is to implement the DQ reconversion period in a fully time-reversed (backwards) fashion. When one $8\tau_{\mathrm{R}}$ cycle is not completed during excitation, the reconversion starts with the incomplete $N\tau_{\mathrm{R}}$ cycle applied backwards. The pulse numbering and the brackets in Fig. 2d emphasize this point. Note that the full DQ experiment includes a preparation step, which is a phase-cycle controlled spin temperature inversion, which doubles the overall phase cycle. This is necessary for samples (such as polymer melts or elastomers), where a rather short T_1 reaches the timescale of the DQ recoupling. Then, additional z magnetization builds up during $2\tau_{\mathrm{DQ}}$, which ends up as additional intensity in the reference signal I_{ref} at long times, preventing proper normalization and, if necessary, tail subtraction. The complete phase cycle

thus has 32 steps (4 for DQ/ref filtering × 4 for CYCLOPS × 2 for inversion). The z filter periods are usually chosen to be 1 ms.

4. Results and discussion

In the following, we demonstrate the performance of BaBa-xy16 on a well studied phosphate sample with small ^{31}P–^{31}P DCC and rather large CSA, employing fast and ultra-fast MAS with frequencies of 30 and 60 kHz, respectively. The experimental findings are compared with detailed spin dynamics simulations, which are also performed for the biologically relevant case of a ^{13}C–^{13}C spin pair in a peptide. ^{1}H DQ MAS NMR applications are then presented for a rigid solid with internal mobility, and soft, mobile elastomers with weak RDCCs. In the latter case, we discuss the issue of (dynamic) inhomogeneity, which can be assessed by fitting I_{nDQ} build-up curves assuming a DCC distribution.

4.1. Pulse sequence performance for weak couplings and large CSA

Magnesium ultraphosphate, MgP_4O_{11}, has a sheet-like structure with phosphate tetrahedra that are edge-connected to 2 (Q^2) or 3 (Q^3) neighboring tetrahedra via oxygen links (see inset of Fig. 6 below). It has 4 crystallographic sites, characterized by rather large CSA with anisotropy values of about 145 ppm (Q^3) and 173 ppm (Q^2). At 600 MHz ^{1}H Larmor frequency, which is about 243 MHz for ^{31}P, this corresponds to $\delta_{CSA}/2\pi = 35$–42 kHz (the span of the static tensor being 1.5 times larger). With about 2.9 Å distance at closest approach, the ^{31}P–^{31}P DCCs are about 800 Hz.

Fig. 3a shows reference and DQ-filtered (DQF) spectra, the latter being compared with the original "broadband" BaBa, which exhibits a roughly 3–4 times reduced efficiency under the given conditions. As an example for the intensity normalization approach, one may just compare the reference and DQF spectra, the latter carrying about half the intensity. The sum of both spectra represents the remaining sample signal after the given τ_{DQ}. From these numbers, we estimate an nDQ intensity of about 30%.

Fig. 3b and c demonstrate the broadband behavior, with offsets of 10 and 20 kHz being easily tolerated at 30 and 60 kHz MAS, respectively. Obviously, faster spinning, being accompanied by shift refocussing on a shorter timescale due to the decreased cycle length, improves the performance of the sequence. Finally in

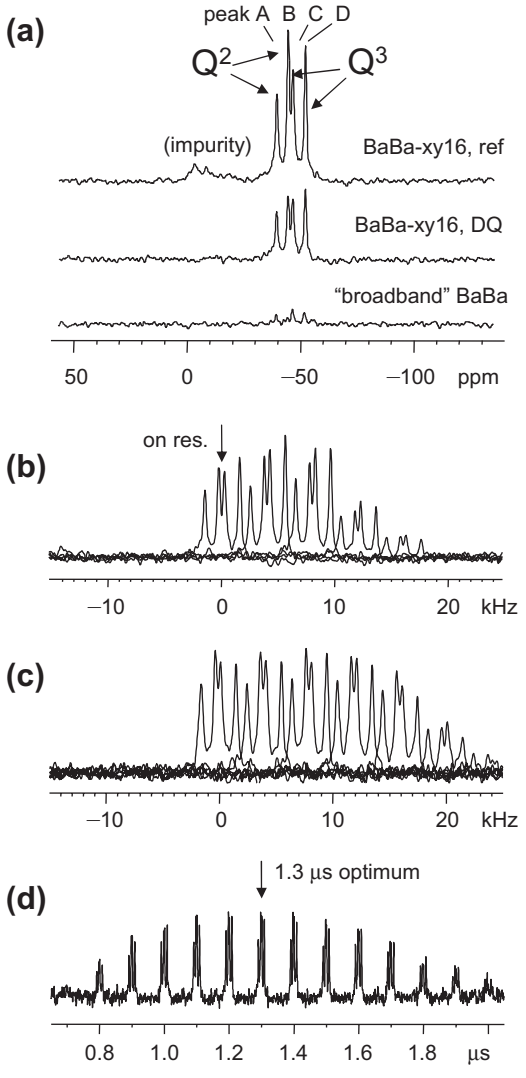

Fig. 3. ^{31}P MAS spectra of MgP_4O_{11} at (a and b) 30 and (c and d) 60 kHz MAS, at a fixed τ_{DQ} of 0.533 ms (16 or 32τ_R, respectively) using BaBa-xy16. (a) Reference and DQ-filtered (DQF) spectra, the latter being compared with "broadband" BaBa. (b and c) DQF spectra as a function of resonance offset at 30 and 60 kHz MAS, respectively. (d) DQF spectra as function of pulse length at fixed rf power, with 1.3 µs corresponding to a 90° flip angle.

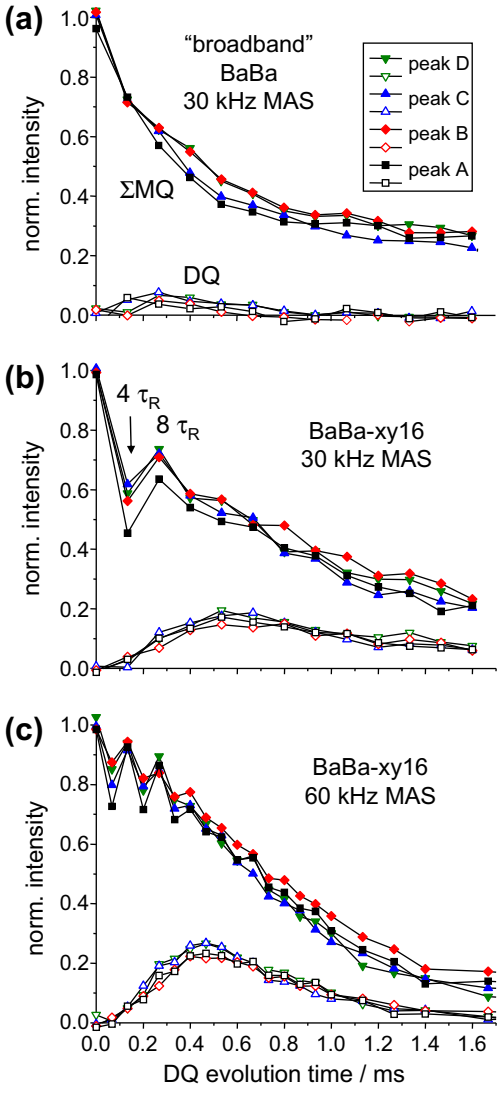

Fig. 4. I_{DQ} build-up (open symbols) and $I_{\Sigma MQ}$ decay data (solid symbols) (a and b) for two different BaBa variants and (b and c) for BaBa-xy16 at two different spinning frequencies for the four distinct resonances A–D. The new sequence is seen to have a roughly 3–4-fold better efficiency.

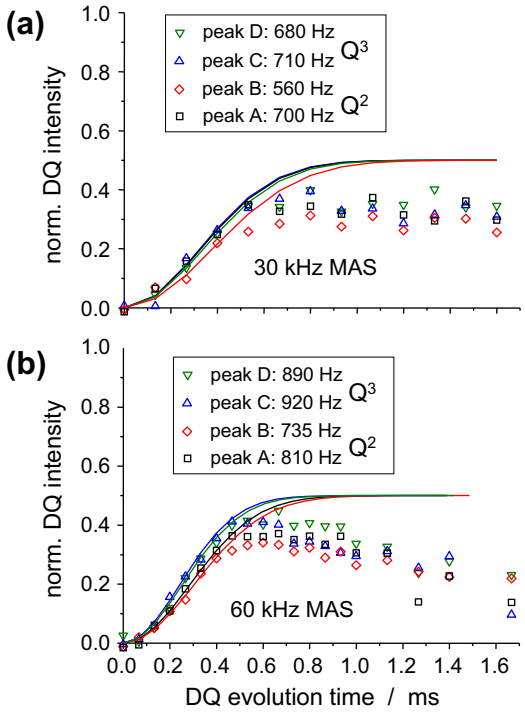

Fig. 5. Normalized build-up functions at (a) 30 and (b) 60 kHz MAS, corresponding to the data in Fig. 4b and c. The solid lines are fits to Eq. (9) using data up to $I_{nDQ} \approx 0.3$, corresponding to the first 4 or 6 data points, respectively. The resulting apparent DCCs ($D_{app}/2\pi$ in Hz) are given in the legends.

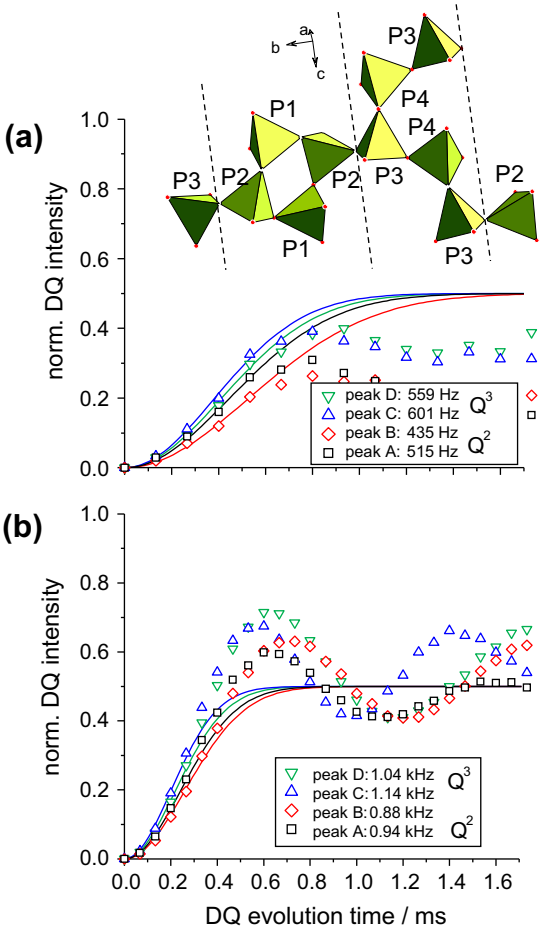

Fig. 6. Computed DQ buildup curves for (a) 30 and (b) 60 kHz MAS, based on the crystal structure of MgP_4O_{11} shown as inset. All ^{31}P sites within a distance of 4.3 Å from the detected spin, about 7–8 spins depending on the site, have been included in the spin dynamics simulations. The solid lines are again fits to Eq. (9) using data up to $I_{nDQ} \approx 0.3$, and the resulting apparent DCCs ($D_{app}/2\pi$ in Hz) are also given.

Fig. 3d, it is shown that even under severely de-tuned conditions, with the flip angle deviating from 90° by up to 30%, the sequence retains its good performance. The similarly favorable dependence on the duty cycle, i.e., the fraction of the rotor period covered by rf irradiation, will be addressed below.

Corresponding I_{DQ} and $I_{\Sigma MQ}$ intensity functions, set to a scale where 1.0 corresponds to the full sample magnetization after a 90° pulse, are plotted in Fig. 4. While the old BaBa has as its only positive feature a rather smooth $I_{\Sigma MQ}$ decay, the DQ excitation efficiency of BaBa-xy16 is again seen to be much more efficient, in particular under ultra-fast MAS conditions where CSA effects are better averaged out. The plots only show excitation times in $4\tau_R$ multiples, and we merely note that the intensity is even more compromised for shorter increments. Perfect compensation is only achieved for the full $8\tau_R$ cycle. However, the decreased intensity at $(8n + 4)\tau_R$ multiples is always reflected in both datasets. Normalized I_{nDQ} build-up data calculated from that data are shown in Fig. 5, where it is seen that the dips in intensity at incomplete cycles are normalized away, leading to rather smooth nDQ build-up data.

Here, we now notice that the data never quite reach the expected intensity plateau of 0.5, indicating still substantial CSA effects on the build-up. Nevertheless, fits based on the second-moment approximation, Eq. (9) are easily possible, and it is seen that the apparent DCCs increase at the faster MAS frequency, indicating better CSA compensation. The fitting results are compared in Table 1 with second-moment predictions based upon the crystal structure (see inset of Fig. 6) , taking into account all ^{31}P spins within 5 Å of the given site. Note that the given numbers have been multiplied by 2/3. This factor arises naturally for the homonuclear DCC between nuclei whose chemical-shift difference is larger than the DCC. This corresponds to the weak coupling limit, analogous to heteronuclear dipole–dipole couplings. Under the given circumstances (tens of kHz CSA), this is realistic, since as soon as the CSA tensors of two given nuclei are not exactly colinear, their effective shift difference is substantial for all possible orientations of the spin pair. This holds as long as the shift refocussing afforded by the pulse sequence ($\sim\omega_R$) is not much faster than the shift frequency difference. The measured values are consistently about 90–95% of

Table 1
^{31}P NMR signals, associated crystallographic sites (see inset of Fig. 6) according to Ref. [36], apparent DCC extracted from the build-up curves at 60 kHz MAS, and second-moment predictions based on the crystal structure, taking into account all ^{31}P spins within 5 Å of the given site.

Signal	Shift (ppm)	Site	Connectivity	$D_{app}/2\pi$ (Hz)	$\frac{2}{3}\left(\sum D_{ij}^2\right)^{1/2}/2\pi$ (Hz)
A	−38.7	P1	Q^2	810	893
B	−43.7	P4	Q^2	735	800
C	−46.1	P2	Q^3	920	980
D	−51.7	P3	Q^3	890	920

the expected values, and the differences between the different sites are more significant than this margin. Thus, our results, obtained on a purely experimental basis of DCCs, confirm the recent assignment [36] that was based on ab-initio calculations of the CSA tensors.

Results of corresponding spin dynamics simulations performed for 600 MHz ^{1}H Larmor frequency are shown in Fig. 6. The simulation results were also fitted to the second-moment-based build-up function, where it is seen that the order of the DCCs associated with the different sites is again in perfect agreement with the known assignment. While the DCC results for 30 kHz MAS are lower than the experimental ones, which is easily explained by the finite number of simulated spins and the correspondingly lower average DCC, the 60 kHz results are larger and also the build-up curves appear irregular in that they exhibit more pronounced oscillations and higher nDQ intensities than expected for a spin pair (see Fig. 1). We leave a clarification of this phenomenon for future work, and tentatively attribute it to a finite spin system size effect. Similar features have also been observed in simulated ^{1}H nDQ build-up data for some specific spin configurations [44]. Overall, the agreement between experimental, simulated, and expected (second-moment DCC estimates) within 20% is gratifying.

The observations and conclusions concerning the robustness of the sequence and the residual CSA effects addressed above are also fully supported by the corresponding spin dynamics simulations shown in Fig. 7. As to the pulse-length and MAS frequency

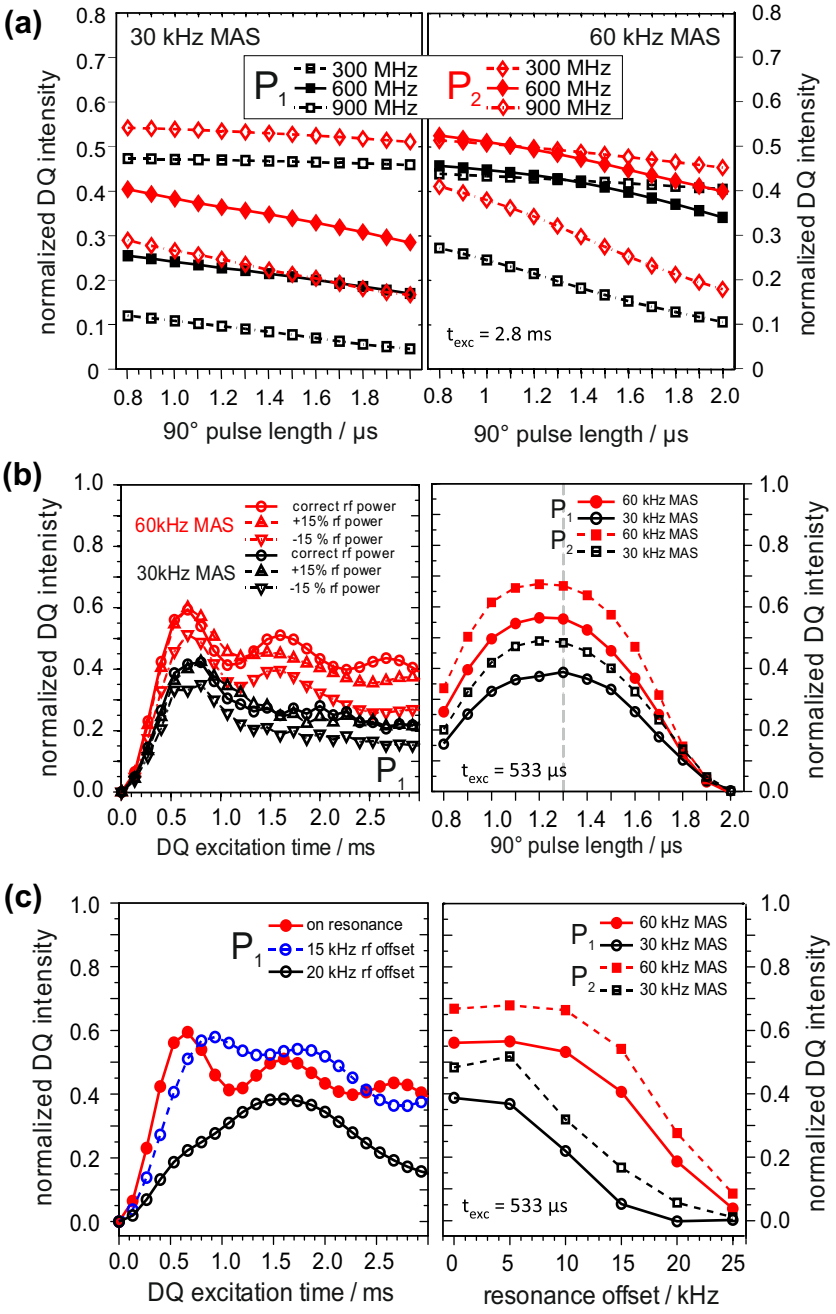

Fig. 7. Simulation results for selected phosphate resonances of MgP_4O_{11}. (a) Both high rf power (corresponding to shorter 90° pulses) as well as fast spinning improve the performance of the pulse sequence. (b) Only severe rf mis-tuning, here simulated for constant nutation frequency (1.3 µs 90° pulse) and variable pulse length, reduces the efficiency of the sequence. (c) BABA-xy16 is well compensated for resonance offsets up to 15 kHz at 60 kHz spinning (left side), and the offset compensation clearly improves with increasing MAS frequency due to the shorter refocusing cycles.

dependence in (a), it is noted that the performance with high rf power or fast spinning alone is not as good as a combination of both. The rather weak effect of mis-tuning on the nDQ build-up is highlighted in (b), where it is seen that deviations towards higher power (flip angles exceeding 90°) are more tolerable. This suggests that for cases of large rf inhomogeneity (full rotors), the best overall flip angle setting is on the order of 100°. The results for the offset dependence shown in (c) are again in good agreement with the corresponding experimental observations in Fig. 3b and c, and demonstrate that large offsets lead to lower apparent DCCs. Even the slight intensity increase at moderate offsets is reproduced. This effect suggests that for large CSA, the best overall DQ efficiency is reached for offset settings closer to the maximum of the corresponding static CSA tensor spectrum rather than the isotropic shift value.

Finally, in order to highlight the potential use of the experiment in biomolecular structure determination, we show in Fig. 8 simulations of the DQ intensity close to the maximum of the build-up curve for the typical case of two amide CO carbons with typical CSA parameters at a distance of 3.3 Å, as found for the closest approach of two amino acids in α-helical conformation. We again address the robustness of the technique with respect to (a) flip angle deviations and (b) resonance offset, both at different spinning frequencies and static field strengths, the latter determining the CSA effect. We again see that the sequence is exceptionally robust with respect to flip angle deviations in particular at lower B_0 fields (lower CSA), but even at the highest field of 800 MHz, deviations on the order of 10% are easily tolerated. This again means that it is not necessary to restrict the sample to the center of the rotor for better rf (B_1) homogeneity. The data (b) is also consistent with the previous observations in that the offset performance improves with faster spinning, and we now also see the magnitude of the CSA does not have a large effect in this case.

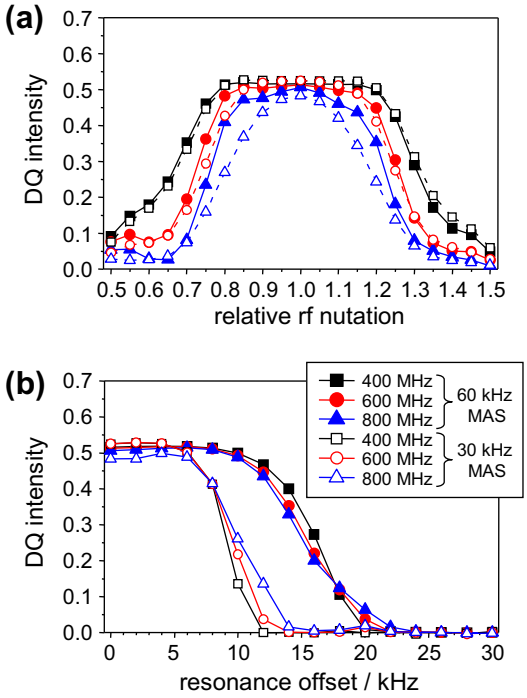

Fig. 8. Simulations demonstrating the performance of BaBa-xy16 in ^{13}C–^{13}C distance determination on the example of the DQ intensity for a pair of amide-CO's with typical CSA parameters ($\delta/(\gamma_C B_0)$ = 85 ppm, η = 0.69) and 3.3 Å distance at 30 and 60 kHz spinning. The simulations are based on a recoupling time of 2.933 ms (88 or 176τ_R, respectively) and a 90° pulse length of 1.6 μs, varying (a) the flip angle as specified relative to the ideal flip angle and (b) the rf offset as given relative to the isotropic shifts.

4.2. Application to strongly coupled ^1H systems with mobility

As a case of rather strong yet motionally averaged ^1H–^1H dipolar couplings, we present data for a PDMS@γ-cyclodextrin inclusion compound. In the cylindrically confined environment provided by the cyclodextrin rings, the highly mobile PDMS chain essentially performs fast (≫100 kHz) uniaxial rotational motions (or a sequence of conformational jumps). In our previous work, which was limited to 30 kHz spinning [24], the intra-CH_3 RDCCs associated with the PDMS resonance were estimated from spinning sidebands using the old BaBa version, and also a heteronuclear variant addressing the ^{13}C–^1H coupling.

The use of BaBa-xy16 at ultra-fast MAS has several advantages. First, the improved spectral resolution of the 2D spectrum in Fig. 9a allows us to conclude that the residual solvent impurity is in fact also confined to the channel structure, as indicated by the corresponding cross-peak. Further, the cross-peak of the PDMS resonance with the host is now well separated and can be integrated and the signal contribution thus quantified (see below). Finally, the improved recoupling time resolution ($2\tau_R$ increments proved feasible) allows for a quantitative analysis of the DQ intensity build-up, see Fig. 9b. As a first step, the ΣMQ decay data, to be used for normalization, shows a long-time exponential tail of about 9% amplitude, which is most likely associated with a corresponding amount of non-included, isotropically mobile PDMS chains. This contribution is thus easily quantified and subtracted.

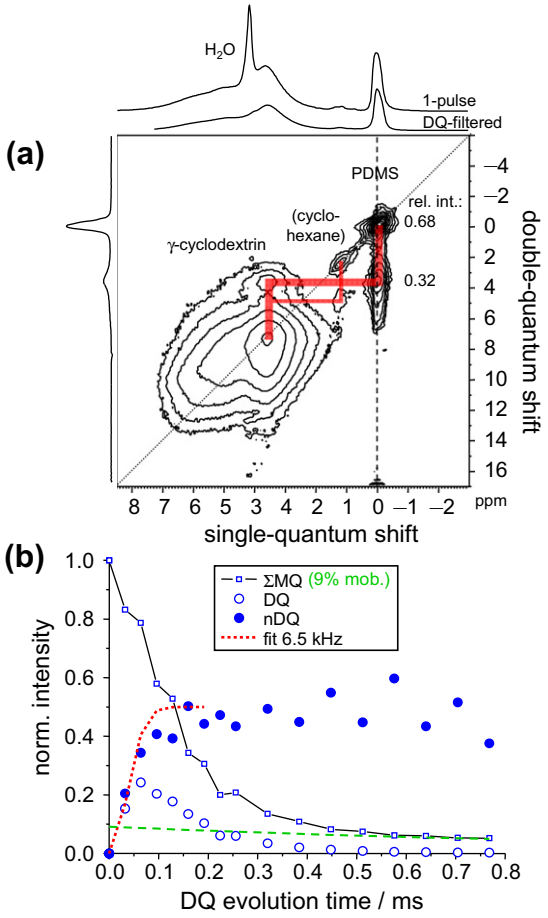

Fig. 9. (a) 2D DQ correlation spectrum (600 MHz) of a PDMS@γ-cyclodextrin inclusion compound at 63 kHz MAS and $\tau_{DQ} = 4\tau_R = 67$ μs. (b) Intensity data for the PDMS resonance in 1D DQF spectra in increments of $2\tau_R$. The dashed line is a fit to the slowly relaxing ΣMQ signal tail corresponding to 9% uncoupled (isotropically mobile) polymer chains.

From the fit to Eq. (9) with only the first 3 points of the resulting nDQ build-up curve, a residual DCC of about 6.5 kHz is easily obtained. Given a motionally averaged RDCC, a dynamic order parameter associated with the backbone motion is obtained as

$$S_b = k\, D_{res}/D_{stat}, \tag{12}$$

where D_{stat}/k is a reference DCC associated here with a fully stretched, rotating PDMS chain. With a reference value for the protons of PDMS of $D_{stat}/(2\pi k)$ = 7.58 kHz obtained from spin dynamics simulations of a suitable model [44], we obtain $S_b \approx 0.86$. This value is yet to be corrected for the influence of couplings to the host. The relative intensity of the intra-PDMS couplings is 0.68 (see Fig. 9a), and since at short recoupling times, $I \propto D^2\tau_{DQ}^2$ (series expansion of the $\sin^2$ dependence in Eq. (4)), we can thus correct S_b simply by multiplication with $\sqrt{0.68}$, which leads to $S_b \approx 0.71$. This result is in good agreement with the value of 0.72 obtained previously from the (more localized) ^{13}C–^1H RDCC [24].

In closing this section, we note that for the given case of still rather strong DCCs, there were still substantial (~30%) intensity losses for recoupling times equal to odd multiples of τ_R. We attribute these to effects of unwanted higher-order contributions to the dipolar Hamiltonian. In the given case, where the MQ reference signal contains the liquid-like impurity signal, proper accounting for and subtracting of the latter was not possible using also the odd increments.

4.3. Application to weakly coupled ^1H systems

4.3.1. Application to homogeneous elastomers and comparison with other pulse sequences

Much previous work of our group was concerned with the precision measurement of ^1H RDCCs is elastomeric materials, for a review see [25]. In elastomers, where the highly mobile polymer chains are fixed at their ends at the chemical crosslink positions, the correspondingly small dynamic chain order parameter S_b (see Eq. (12)) is directly proportional to the density of crosslinks (i.e., it is inversely proportional to the number of monomers in the network chains). Roughly speaking, $S_b \approx 1/N_s$, where N_s is the number of segments of the network chain. Since typically, $N_s \sim 100$, S_b is on the order of 1%. An exact measurement of the weak RDCC is thus highly desirable, as it reflects valuable structural information. Up to now, such studies were limited to simple single-component elastomers with simple monomer units, i.e. those that carry all protons close to the main chain [44]. In such cases, which fortunately cover much of the commercially relevant rubbers, it is sufficient to measure the integral proton signal without chemical resolution under low-resolution (static, and possibly low-field) conditions.

In fact, the static DQ experiment based on a pulse sequence of Baum and Pines (see Fig. 1) as applied to mobile ^1H systems is exceptionally robust, yielding data that hardly depend on the experimental conditions (B_0 field strength and homogeneity, rf performance, etc.). In contrast, the first applications of MAS recoupling sequences to such weakly coupled systems suffered severe imperfection-related intensity losses at the required long recoupling times [45], precluding a quantitative direct analysis of nDQ build-up data. Establishing a robust experiment applicable under MAS conditions was thus highly desirable in view of a now vastly enlarged application range. We thus highlight the application of BaBa-xy16 to rubbery systems focussing first on a model elastomer without substantial inhomogeneities (NR), and on a more complex one where chemical shift selectivity is essential (PMA).

The 2D DQ shift correlation spectrum in Fig. 10 highlights the advantages of high-resolution MAS spectroscopy of elastomeric materials, as pioneered in Ref. [45]: All cross-peaks between the different protons are resolved, and an analysis of their relative

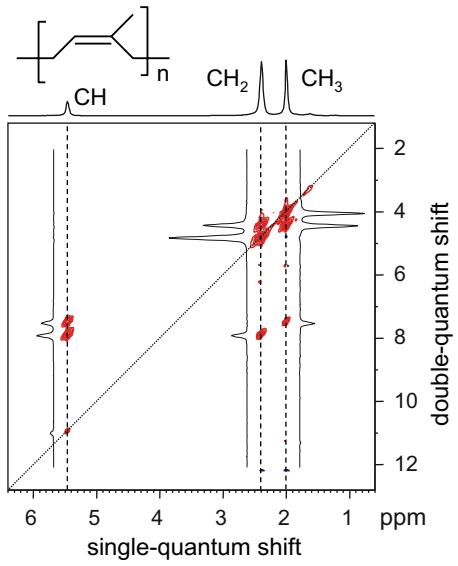

Fig. 10. 2D DQ correlation spectrum (400 MHz) of NR at 10 kHz MAS, 75 °C sample temperature and $\tau_{DQ} = 8\tau_R = 0.8$ ms, including a projection along the SQ dimension (top) and 1D slices along the DQ dimension.

intensities, taken from slices along the DQ dimension, can be a basis for a derivation of suitable models for the geometry of the fast conformational dynamics [45]. Ensuing, more detailed work was limited to the analysis of the combined aliphatic and olefinic resonances that are resolved in static spectra [44]. A notable result from our previous work was that the nDQ build-up curves taken from 1D DQF spectra at the two distinguishable resonances are almost identical, which is an *a priori* unexpected finding noting that the olefinic CH proton appears rather isolated. The reason is of course to be sought in the geometry of fast local motions, that for instance rather effectively average the intra-CH_2 coupling due to its specific internuclear orientation with respect to the symmetry axis of motion.

Intensity data obtained using BaBa-xy16 are plotted in Fig. 11 and highlight the good long-time performance of the sequence. In (a), all data points in $1\tau_R$ increments are now shown. Again, higher-order effects lead to intensity reductions on the order of 10% for recoupling times unequal to $4N\tau_R$, however, these oscillations are removed completely upon calculating the nDQ build-up data. The resulting curve is exceptionally smooth and allows for in-depth analyses based on heterogeneous models assuming RDCC distributions [25,33,46]. Elastomers are expected to be heterogeneous by way of their preparation, where the vulcanization (or cross-linking) agents may well be distributed inhomogeneously upon processing, which means that the locally detected cross-link density, as reflected in a specific RDCC, may vary in space.

The shape of the nDQ build-up curve in the given example deserves some comments. It exhibits a slight maximum before nicely levelling out at the expected intensity plateau of 50%. While one may be tempted to attribute it to the oscillations arising from the powder average in the spin-pair limit (see Fig. 1), earlier static spin counting experiments have proven that it rather arises from multiple-quantum dynamics [33]. This means that around the maximum of the actual 2-quantum build-up, the growing importance of 4-quantum coherences that contribute to the reference intensity, lead to the observed decay. Further oscillations due to higher quantum orders are invisible due to their low intensity. Recent work of our group has shown that the observed shape of the nDQ build-curve is in fact generic in that it does not depend on the specific type of elastomer as long as the polymer consists of "simple" monomer units with all protons closely linked to the

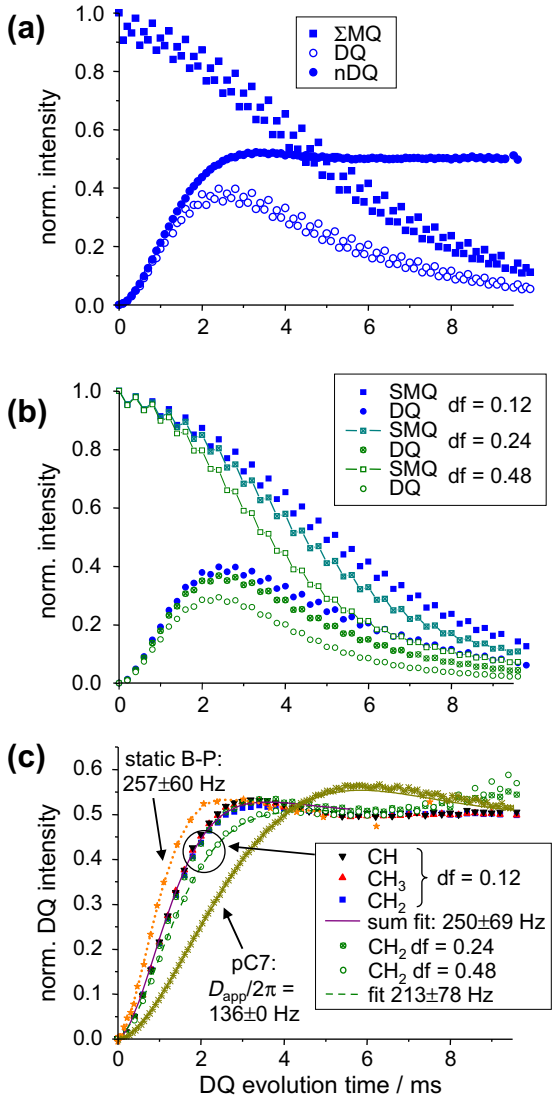

Fig. 11. ΣMQ decay, as well as DQ and nDQ build-up intensities for NR taken under the same conditions as given in Fig. 10. (a) ΣMQ, DQ and nDQ data for the CH_2 resonance, showing τ_{DQ} increments of $1\tau_R$. (b) ΣMQ and DQ intensities for the CH_2 group, showing only $2\tau_R$ increments for clarity, varying the 90° pulse length (3, 6, and 12 μs) resulting in different rf duty factors (df). (c) nDQ build-up curves for all three resonances (including the three different duty cycle values for the CH_2 case) and (combined) fits based on Eqs. (13) and (14) assuming a Gaussian distribution of RDCCs. The standard deviation (width) of the distribution is indicated after the ± sign. These data are compared to the results of a static MQ experiment and pC7, the latter being a weighted average of all three resonances, taken at 8164 Hz spinning and the correspondingly required rf power, as optimized on the sample.

main chain. Such a multi-spin system without clear hierarchies in next-neighbor couplings thus exhibits a homogeneous response function.

Using chemically different yet very homogeneous model elastomers with negligible RDCC distribution, it was possible to find an analytical representation of the generic build-up function,

$$I_{nDQ}(\tau_{DQ}, D_{res}) = 0.5(1 - \exp\left\{-\left(0.378\epsilon D_{res}\tau_{DQ}\right)^{1.5}\right\} \times \cos(0.583\epsilon D_{res}\tau_{DQ})), \quad (13)$$

where the prefactor $\epsilon_{stat} = 1$ for the static (Baum–Pines) MQ experiment, and $\epsilon_{Baba} = 0.78$ for BaBa-xy16 with its slightly reduced efficiency. This function serves as basis for the analysis of the RDCC distribution $f(D_{res})$, for which the integral sample response is given by

$$g(\tau_{DQ}) = \int_0^\infty K[D_{res}, \tau_{DQ}] f(D_{res}) \mathrm{d}D_{res}. \quad (14)$$

Using Eq. (13) as Kernel function $K[D_{res}, \tau_{DQ}]$, the (ill-posed) problem of inverting the above integral equation can be solved numerically, as discussed in detail in Ref. [46]. As an simple alternative, one can assume $f(D_{res})$ to be a Gaussian distribution with average RDCC D_{av} and width σ. For such a simple model, fits with Eq. (14) can be implemented numerically, with a finite-step integration extending over about $D_{res} = \pm 5\sigma$.

Turning back to the given NR rubber sample, we first note the duty cycle (pulse length) dependence shown in Fig. 11b. It is seen that the DQ efficiency is visibly compromised only beyond a duty cycle of 25%. In Fig. 11c, the nDQ build-up curves for all 3 resonances are plotted, and they are seen to be equal within the experimental accuracy. This again validates the statements made on the homogeneous spin dynamics in the monomer unit of NR. A combined fit to Eqs. (13) and (14) yields an average RDCC of 250 Hz and a distribution width of 69 Hz. The MAS data in Fig. 11c are compared to those of a static experiment performed at low field (20 MHz, Bruker minispec), which gives virtually the same results, with the visible difference that the static MQ sequence has a higher scaling factor, as discussed in the context of Fig. 1. This finding constitutes the justification to use Eq. (13), which was developed for the static case, also for BaBa-xy16.

We conclude this part by emphasizing that good-quality DQ and ΣMQ curves, offering the required stability at long recoupling times, are readily obtained with the static pulse sequence and with BaBa-xy16, while good stability, in particular needed to record the ΣMQ signal to long times suitable for tail fitting, was far from easy to achieve with pC7, data for which are also included in Fig. 11c. Here, we fitted again to Eqs. (13) and (14) using $\epsilon_{Baba} = 0.78$. The difference in the average RDCC thus simply reflects the lower scaling factor of pC7. Notably however, the fact that the fitted apparent distribution width σ was zero indicates that the generic shape of the pC7 build-up is slightly different from the static and BaBa cases. In fact, the local maximum is a bit higher, possibly as a consequence of the rather different orientation angle dependence of its Hamiltonian. The difference is, however, rather minor.

In the pC7 case, it must be stressed that for acceptable results the rf set-up had to be carefully optimized on the actual sample, and we had to invest in the new Bruker HPLNA pre-amplifier to ensure good long-time high-power ^{1}H rf performance. In contrast for BaBa-xy16, sub-optimal tune-up conditions are tolerable, yet in such a case, good-quality imperfection compensation is only achieved every $4\tau_R$, reducing the number of usable build-up points. In this regard, a well-tuned pC7 offers the possibility of very small time increments ($2/7\tau_R$), providing many more data points. Note that for increments $N2/7\tau_R$ when $N \neq 7$, the base phase of the pC7 reconversion must be rotated by the corresponding fraction of 360° to achieve proper DQ reconversion since the excited DQ coherence carries a corresponding phase shift.

4.3.2. Application to chemically complex and inhomogeneous elastomers

We finally turn to a more complex case, focussing on elastomers made from chains where the monomer unit has a stereo center and/or longer side groups. In such cases, main- and side-chain protons can be partially dynamically decoupled, or different stereo sequences may exhibit different motional geometries, which means that it is conceivable that the RDCCs detected at the different resonances can be different. The results shown for the PMA network in Fig. 12 confirm this statement.

To the best of our knowledge, there is no published validated assignment of the different ^{1}H resonance positions of PMA; the assignment shown in Fig. 12a is taken from refs. [47,48], and is

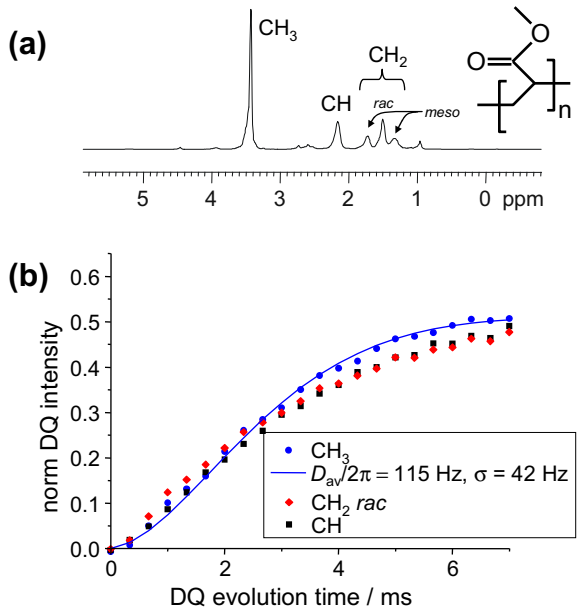

Fig. 12. Results for the partially swollen PMA network sample, taken at 6 kHz MAS and 100°C sample temperature for sufficiently fast segmental mobility. (a) 1D spectrum with chemical structure assignments, (b) nDQ build-up curves taken at three different resonance positions, with a fit to the CH_3 data based on Eqs. (13) and (14) assuming a Gaussian distribution of RDCCs.

probably based on comparisons with other (meth)acrylates. Most notably, signals of seemingly equivalent CH_2 protons appear multiply at different spectral positions reflecting their origin in *meso* or *racemic* stereochemical monomer diads, where in the former, the two protons are in fact inequivalent. This is a consequence of the sensitivity of the chemical shift to different time-averaged chain conformations, as also observed for many other polymers [49]. PMA synthesized by radical polymerization is an atactic polymer, where the averaged conformational states (and thus the isotropic shift and the time-averaged RDCC) depend on the stereochemistry of neighboring monomer units. The nDQ build-up curves plotted in Fig. 12b detected at the resonance positions for $CH_{2,rac}$ and CH appear even slightly bimodal, with a quicker initial rise and a delayed long-time build-up. This corroborates that the stereochemistry of even longer monomer sequences, that are not distinguished in the ^{1}H resonances (but in the ^{13}C resonances [47]) is associated with a variability in the local dynamics and thus in the local RDCCs. It is clear that an RDCC distribution analysis of the integral spectral response would superficially imply a rather inhomogeneous elastomer.

Obviously however, the build-up curve detected at the CH_3 position, corresponding to the dynamically decoupled methoxy side chain, is almost monomodal and can be fitted to a well-defined average RDCC with a standard deviation of only 37% of the average. Obviously, the geometry of the trajectory of the outer O–CH_3 bond (that ultimately determines the intra-CH_3 RDCC) is less dependent on the stereosequence. So the investigated sample is indeed rather homogeneous, as it is in fact expected from its preparation from well-defined star-shaped precursors. A systematic study of the (in)homogeneity of such model networks, exhibiting local "spin complexity" as a simple result of the monomer unit structure, is thus only possible with suitable high-resolution MAS DQ experiments.

As a final note concluding this section on elastomer applications, we stress that a deformation of the samples inside the spinning rotor must be avoided as completely as possible. If the samples are compressed (=stretched biaxially) as a result of centrifugal forces, the network chains become oriented, which increases not only the average RDCC, but also changes the orientation distribution of the RDCC tensor – the sample becomes partially ordered on a macroscopic scale. This leads to build-up curves with more pronounced maxima that cannot be fitted to Eq. (9) or (13). Possible strategies to avoid these complications are the use of perfectly cylindrical samples that fill the complete rotor and do not have space to deform, or to stick to lower MAS frequencies.

5. Conclusions

In summary, we have shown that BaBa-xy16 ranks among the most efficient, broadband DQ recoupling pulse sequences available, being applicable to a wide range of nuclei and MAS frequencies. Its advantages are its robustness with respect to rf setup accuracy and overall power requirement, its comparably low duty cycle (only one 360° nutation per rotor cycle), and its broadband behavior in particular at the highest MAS frequencies available, making it very user-friendly. Its limits are certainly the applicability to CSA or offset frequencies reaching or even exceeding the available MAS frequency, as often found in ^{19}F NMR, and the fact that in systems with large offsets/CSAs or dipole–dipole couplings, good imperfection compensation is only achieved for DQ build-up times of $N \times 4$ rotor periods. Very reliable build-up data using single rotor-period increments can however be obtained in soft-matter systems. We have demonstrated for elastomers that DQ-build curves can be measured that can be quantitatively analyzed not only in terms of an average coupling constant, but also in terms of coupling distributions, as found in dynamically heterogeneous systems such as chemically or spatially inhomogeneous rubbers.

While weak dipole–dipole couplings are best extracted from normalized DQ build-up curves, we stress that strong couplings, for which only a few data points in the meaningful initial DQ build-up region may be available, are better determined by spinning sideband analysis. This means that an optional t_1 DQ evolution time is inserted between DQ excitation and reconversion of fixed length. Incrementing t_1 in steps of a small fraction of the rotor period leads to a spinning sideband pattern in the indirect (DQ) spectral dimension of the resulting 2D DQ–SQ correlation spectrum that directly reflects the coupling constant [50,51]. The basic principles and numerous applications of this concept have been published by Schnell and Spiess [18] and Brown and Spiess [19], and along with the improved protocol published here, we expect many more fruitful applications of BaBa-xy16.

We finally note that γ-encoded DQ recoupling sequences such as pC7 [7] do not offer the potential for sideband analysis [5,52], and remind also that the frequently emphasized, potentially better DQ efficiency of such sequences due to the different orientation dependence is often not realized in actual experiments, in particular in systems with multiple coupled spins, whose DQ build-up behavior is dominated by spin dynamics involving higher-order coherences. Here, we have demonstrated that in multi-spin systems, the DQ build-up follows a rather generic second-moment-type behavior, whose functional form is virtually identical for the static case and MAS with BaBa-xy16, and still rather similar for pC7.

Acknowledgments

We thank Hans Förster (Bruker Biospin) for many invaluable discussions over the years and his as well as Walter Chassé's help in setting up pC7 on our spectrometers, S. Ebbinghaus for supplying the cif file for the magnesium ultraphosphate, D. Huster for advice on peptide CSA tensors, and Jörn Schmedt auf der Günne for discussions concerning CSA tensor orientations in phosphates.

Funding of this work was partially provided by the DFG (SA982/7-1). Infrastructure support from the European Union (ERDF programme) is gratefully acknowledged.

Appendix A. Supplementary material

Pulse sequences (Bruker Avance III) for build-up analysis and 2D DQ-SQ correlation spectra used in this article can be found in the online version, at doi:10.1016/j.jmr.2011.07.001.

References

[1] R.R. Ernst, G. Bodenhausen, A. Wokaun, Principles of Nuclear Magnetic Resonance in One and Two Dimensions, Clarendon Press, Oxford, 1987.
[2] R. Tycko, G. Dabbagh, Measurement of nuclear magnetic dipole–dipole couplings in magic angle spinning NMR, Chem. Phys. Lett. 173 (1990) 461–465.
[3] S. Dusold, A. Sebald, Dipolar recoupling under magic-angle spinning conditions, Ann. Rep. NMR Spectrosc. 41 (2000) 185–264.
[4] M. Carravetta, M. Edén, X. Zhao, A. Brinkmann, M.H. Levitt, Symmetry principles for the design of radiofrequency pulse sequences in the nuclear magnetic resonance of rotating solids, Chem. Phys. Lett. 321 (2000) 205–215.
[5] M.H. Levitt, Symmetry-based pulse sequences in magic-angle spinning solid-state NMR, in: D.M. Grant, R.K. Harris (Eds.), Encyc. Nucl. Magn. Reson, vol. 9, John Wiley & Sons, Chichester, 2002, pp. 165–196.
[6] Y.K. Lee, N.D. Kurur, M. Helmle, O.G. Johannessen, N.C. Nielsen, M.H. Levitt, Efficient dipolar recoupling in the NMR of rotating solids. A sevenfold symmetric radiofrequency pulse sequence, Chem. Phys. Lett. 242 (1995) 304–309.
[7] M. Hohwy, H.J. Jakobsen, M. Edén, M.H. Levitt, N.C. Nielsen, Broadband dipolar recoupling in the nuclear magnetic resonance of rotating solids: a compensated C7 pulse sequence, J. Chem. Phys. 108 (1998) 2686–2694.
[8] Y. Ishii, ^{13}C–^{13}C dipolar recoupling under very fast magic angle spinning in solid-state nuclear magnetic resonance: applications to distance measurements, spectral assignments, and high-throughput secondary-structure determination, J. Chem. Phys. 114 (2001) 8473–8483.
[9] N.A. Oyler, R. Tycko, Multiple-quantum ^{13}C NMR spectroscopy in solids under high-speed magic-angle spinning, J. Phys. Chem. B 106 (2002) 8382–8389.
[10] B. Hu, Q. Wang, O. Lafon, J. Trébosc, F. Deng, J.P. Amoureux, Robust and efficient spin-locked symmetry-based double-quantum homonuclear dipolar recoupling for probing ^{1}H–^{1}H proximity in the solid-state, J. Magn. Reson. 198 (2009) 41–48.
[11] B. Hu, L. Delevoye, O. Lafon, J. Trébosc, J.P. Amoureux, Double-quantum NMR spectroscopy of ^{31}P species submitted to very large CSAs, J. Magn. Reson. 200 (2009) 178–188.
[12] Q. Wang, B. Hu, O. Lafon, J. Trébosc, F. Deng, J.-P. Amoureux, Homonuclear dipolar recoupling under ultra-fast magic-angle spinning: probing ^{19}F–^{19}F proximities by solid-state NMR, J. Magn. Reson. 203 (2010) 113–128.
[13] Y.-H. Tseng, Y. Mou, C.-Y. Mou, J.C.C. Chan, Double-quantum NMR spectroscopy based on finite-pulse RFDR, Solid State Nucl. Magn. Reson. 27 (2005) 266–270.
[14] C. Kehlet, T. Vosegaard, N. Khaneja, S.J. Glaser, N.C. Nielsen, Low-power homonuclear dipolar recoupling in solid-state NMR developed using optimal control theory, Chem. Phys. Lett. 414 (2005) 204–209.
[15] Z. Tošner, S.J. Glaser, N. Khaneja, N.C. Nielsen, Effective Hamiltonians by optimal control: solid-state NMR double-quantum planar and isotropic dipolar recoupling, J. Chem. Phys. 125 (2006) 184502.
[16] M.J. Bayro, M. Huber, R. Ramachandran, T.C. Davenport, B.H. Meier, M. Ernst, R.G. Griffin, Dipolar truncation in magic-angle spinning NMR recoupling experiments, J. Chem. Phys. 130 (2009) 114506.
[17] M. Feike, D.E. Demco, R. Graf, J. Gottwald, S. Hafner, H.W. Spiess, Broadband multiple-quantum NMR spectroscopy, J. Magn. Reson. A 122 (1996) 214–221.
[18] I. Schnell, H.W. Spiess, High-resolution ^{1}H NMR spectroscopy in the solid state: very-fast sample rotation and multiple-quantum coherences, J. Magn. Reson./Adv. Magn. Reson. 151 (2001) 153–227.
[19] S.P. Brown, H.W. Spiess, Advanced solid-state NMR methods for the elucidation of structure and dynamics of molecular, macromolecular, and supramolecular systems, Chem. Rev. 101 (2001) 4125–4155.
[20] M. Feike, R. Graf, I. Schnell, C. Jäger, H.W. Spiess, Structure of crystalline phosphates from ^{31}P double-quantum NMR spectroscopy, J. Am. Chem. Soc. 118 (1996) 9631–9634.
[21] F.-C. Chou, T.W.T. Tsai, H.-K. Lee, J.C.C. Chan, Compensated DRAMA sequence for homonuclear dipolar recoupling under magic-angle spinning, Solid State Nucl. Magn. Reson. 36 (2009) 177–181.
[22] T. Gullion, D.B. Baker, M.S. Conradi, New, compensated Carr-Purcell sequences, J. Magn. Reson. 89 (1990) 479–484.
[23] J. Schmedt auf der Günne, Distance measurements in spin-1/2 systems by ^{13}C and ^{31}P solid-state NMR in dense dipolar networks, J. Magn. Reson. 165 (2003) 18–32.
[24] K. Saalwächter, An investigation of poly(dimethylsiloxane) Chain dynamics and order in its inclusion compound with γ-cyclodextrin by fast-MAS solid-state NMR spectroscopy, Macromol. Rapid. Commun. 23 (2002) 286–291.
[25] K. Saalwächter, Proton multiple-quantum NMR for the study of chain dynamics and structural constraints in polymeric soft materials, Progr. NMR Spectrosc. 51 (2007) 1–35.
[26] J.L. Valentín, J. Carretero-González, I. Mora-Barrantes, W. Chassé, K. Saalwächter, Uncertainties in the determination of cross-link density by equilibrium swelling experiments in natural rubber, Macromolecules 41 (2008) 4717–4729.
[27] K. Matyjaszewski, J. Xia, Atom transfer radical polymerization, Chem. Rev. 101 (2001) 2921–2990.
[28] J.A. Johnson, D.R. Lewis, D.D. Díaz, M.G. Finn, J.T. Koberstein, N.J. Turro, Synthesis of degradable model networks via ATRP and click chemistry, J. Am. Chem. Soc. 128 (2006) 6564–6565.
[29] H. Gao, K. Matyjaszewski, Synthesis of functional polymers with controlled architecture by CRP of monomers in the presence of cross-linkers: from stars to gels, Prog. Polym. Sci. 34 (2009) 317–350.
[30] K. Matyjaszewski, N.V. Tsarevsky, Nanostructured functional materials prepared by atom transfer radical polymerization, Nat. Chem. 1 (2009) 276–288.
[31] A.J. Brandolini, D.D. Hills, NMR Spectra of Polymers and Polymer Additives, Marcel Dekker, Basel, 2000.
[32] J. Baum, A. Pines, NMR studies of clustering in solids, J. Am. Chem. Soc. 108 (1986) 7447–7454.
[33] K. Saalwächter, P. Ziegler, O. Spyckerelle, B. Haidar, A. Vidal, J.-U. Sommer, ^{1}H multiple-quantum nuclear magnetic resonance investigations of molecular order distributions in poly(dimethylsiloxane) networks: evidence for a linear mixing law in bimodal systems, J. Chem. Phys. 119 (2003) 3468–3482.
[34] M. Veshtort, R.G. Griffin, SPINEVOLUTION: a powerful tool for the simulation of solid and liquid state NMR experiments, J. Magn. Reson. 178 (2006) 248–282.
[35] D. Stachel, H. Paulus, C. Guenter, H. Fuess, Crystal structure of magnesium ultraphosphate, MgP_4O_{11}, Z. Kristallogr. 199 (1992) 275–276.
[36] J. Weber, J. Schmedt auf der Günne, Calculation of NMR parameters in ionic solids by an improved self-consistent embedded cluster method, Phys. Chem. Chem. Phys. 12 (2010) 583–603.
[37] J. Weber, J. Schmedt auf der Günne, personal communication, 2010.
[38] J. Baum, M. Munowitz, A.N. Garroway, A. Pines, Multiple-quantum dynamics in solid state NMR, J. Chem. Phys. 83 (1985) 2015–2025.
[39] T. Gullion, J. Schaefer, Rotational-echo double-resonance NMR, J. Magn. Reson. 81 (1989) 196–200.
[40] P.W. Anderson, P.R. Weiss, Exchange narrowing in paramagnetic resonance, Rev. Mod. Phys. 25 (1953) 269–276.
[41] R. Kimmich, NMR Tomography, Diffusometry, Relaxometry, Springer, Berlin, 1997.
[42] K. Saalwächter, A. Heuer, Chain dynamics in elastomers as investigated by proton multiple-quantum NMR, Macromolecules 39 (2006) 3291–3303.
[43] F. Vaca Chávez, K. Saalwächter, Time-domain NMR observation of entangled polymer dynamics: analytical theory of signal functions, Macromolecules 44 (2011) 1560–1569.
[44] K. Saalwächter, B. Herrero, M.A. López-Manchado, Chain order and crosslink density of elastomers as investigated by proton multiple-quantum NMR, Macromolecules 38 (2005) 9650–9660.
[45] R. Graf, A. Heuer, H.W. Spiess, Chain-order effects in polymer melts probed by ^{1}H double-quantum NMR spectrocopy, Phys. Rev. Lett. 80 (1998) 5738–5741.
[46] W. Chassé, J.L. Valentín, G.D. Genesky, C. Cohen, K. Saalwächter, Precise dipolar coupling constant distribution analysis in proton multiple-quantum NMR of elastomers, J. Chem. Phys. 134 (2011) 044907.
[47] J.-S. Wang, K. Matyjaszewski, Controlled/"living" radical polymerization. Halogen atom transfer radical polymerization promoted by a Cu(I)/Cu(II) redox process, Macromolecules 28 (1995) 7901–7910.
[48] I.D. Cunningham, K. Fassihi, The cyclopentadienyltitanium trichloride/MAO-catalysed polymerization of methyl acrylate and copolymerisation with styrene and isoprene, Polym. Bull. 53 (2005) 359–365.
[49] A.E. Tonelli, NMR Spectroscopy and Polymer Microstructure: The Conformational Connection, VCH, Weinheim, 1989.
[50] H. Geen, J.J. Titman, J. Gottwald, H.W. Spiess, Spinning sidebands in the fast-MAS multiple-quantum spectra of protons in solids, J. Magn. Reson. A 114 (1995) 264–267.
[51] J. Gottwald, D.E. Demco, R. Graf, H.W. Spiess, High-resolution double-quantum NMR spectroscopy of homonuclear spin pairs and proton connectivities in solids, Chem. Phys. Lett. 243 (1995) 314–323.
[52] G. Pileio, M. Concistrè, N. McLean, A. Gansmüller, R.C.D. Brown, M.H. Levitt, Analytical theory of γ-encoded double-quantum recoupling sequences in solid-state nuclear magnetic resonance, J. Magn. Reson. 186 (2007) 65–74.